

## **Influence of High Temperature, Stress and Chloride Ions on Protection Mechanism of Passive Film on 304 Stainless Steel**

Shanlin He<sup>1,\*</sup>, Daming Jiang<sup>1</sup>

School of Materials Science and Engineering, Harbin Institute of Technology, Harbin 150001, China

\*E-mail: [11B909025@hit.edu.cn](mailto:11B909025@hit.edu.cn)

Received: 24 January 2018 / Accepted: 6 March 2018 / Published: 10 April 2018

---

X-ray photoelectron spectroscopy (XPS), atomic force microscopy (AFM) and electrochemical impedance spectroscopy (EIS) were used to analyze the changes in content of chemical compounds, surface morphology and electrochemical properties of the passive film on 304 stainless steel under the combined effect of high temperature, stress and Cl<sup>-</sup>. The protection mechanism of the passive film was investigated. The results showed that the content of chemical compounds experienced changes at different immersion conditions. With increasing immersion time, the ratio between each oxide would level off at different stable values for each immersion condition. The passive film at the surface of the grain boundary was damaged due to the dissolution of chemical compounds. When the surface morphology was damaged, the concentration of the Cr<sub>2</sub>O<sub>3</sub> can not accurately reflect the corrosion resistance of the passive film. The decrease in the corrosion resistance of the passive film was mainly attributed to the corrosion groove, which was formed from the dissolution of the passive film on the surface of the grain boundary.

---

**Keywords:** combined effect; surface morphology; corrosion groove; dissolution; corrosion resistance

### **1. INTRODUCTION**

Because of its excellent corrosion resistance, 304 stainless steel has been widely used in many areas of industrial production [1-8]. The corrosion resistance of stainless steel is due to the dense passive film on its surface [9-15]. The environmental temperature, surface condition, corrosion ions, pH and many other factors all play a big role in the property of the passive film [16-18]. However, materials often experience the combined impact of high temperature, large deformation and even erosive ions in working conditions simultaneously. The harsh working conditions will severely damage the protection performance of passive films, thus resulting in the damage of materials and the occurrence of safety accidents. A series of past research shows that the structure of the passive film consists of an oxide-containing inner layer and a hydroxide-containing outer layer [8-12]. The oxide

layer further consists of a Cr oxide layer and a Fe oxide layer [15-17]. The films exhibit different electrochemical characteristics in different environments [18]. According to the point defect model (PDM), the adsorption of Cl<sup>-</sup> to the oxygen vacancy at the interface of the film and solution can result in the generation of more cation vacancy and oxygen vacancy, destroying the stability of passive films. In Cl<sup>-</sup>-containing solution, the passive film on 304 stainless steel exhibits N-type semiconductor characteristics and contains many defects [19,20]. At high temperature and in a water environment, the protection performance of passive films is mainly controlled by the Cr-rich inner oxide layer [21]. Ferreira found that temperature can cause changes to the amount of inner layer oxide and thus the thickness of the passive film [22]. Kuang found that the pre-formed hematite oxide changes with changing environment [23]. Bojinov found that the diffusion coefficient of passive films immersed for a very long time (72 h) is orders of magnitude lower than that at the beginning of oxidation (<24 h) [24]. Therefore, predicting the long-term protection performance of passive films based on the performance at the beginning of immersion is not appropriate [24-29]. Long-term monitoring is required in order to gain a more accurate understanding of this resistance. Researchers have also investigated the effect of oxidizer concentration [30-33], pH [34], temperature [35,36] and various ions [37-43] on the corrosion behaviors of materials.

However, there are very few studies on the protection mechanism of passive films under the combined effect of many factors. The evolution of the property of passive films is more complicated under complicated conditions, the combined effect is not just a simple addition of the effect of each factor. In addition, some studies focused on the impact of the changes in the content of chemical compounds in the passive film on its protection performance, and the analysis did not take into account of the surface morphology. The corrosion and damage of materials often occur under the combined effect of many factors. Therefore, an in-depth investigation of the protection mechanism of passive films under the combined effect of many factors is of paramount importance.

In the present study, we investigated the evolution of the protection performance of passive film on 304 stainless steel under the combined effect of high temperature, stress and chloride ions. Through the multifactor design of the experimental parameters with different temperature (high temperature and room temperature), loading condition (stress and stress-free) and Cl<sup>-</sup> concentration (sodium chloride solution and deionized water), for the passive film, this research found and further characterised the direct corresponding relation among the surface morphology, chemical composition and corrosion resistance by comparing the results obtained from the methods of atomic force microscope, X-ray photoelectron spectroscopy and electrochemical impedance spectroscopy, and then performed an in-depth analysis of the protection mechanism of the passive film. Under the combined effect of high temperature, stress and chloride ions, the experimental condition in this study was close to the actual service environment of the material, and the results can be useful for studying the corrosion behavior and prevention technology of 304 stainless steel.

## 2. EXPERIMENTAL

A 1 mm-thick 304 stainless-steel sheet was used in the experiments. Its chemical composition is listed in Table 1. First, the sample required solution treatment. The sample was heated to 1050°C

and held for 30 min before air cooling to room temperature. The solution-treated sample was polished with metallographical sand paper and then cleaned with deionized water. After drying, the sample was treated with a pickling process so that a stable passive film was formed on its surface. The pickling solution was composed of 20% nitric acid (density of 1420 kg/m<sup>3</sup>), 5% hydrofluoric acid and 75% water. Pickling lasted for 25 minutes.

**Table 1.** Chemical composition of 304 stainless steel (wt.%).

C	Si	Mn	P	S	Ni	Cr	Fe
0.07	0.46	0.78	0.029	0.006	8.06	18.16	Balance

A cantilever-type sample was used in the immersion experiment. The sample was cut to equal-strength sections, as shown in Figure 1. Under constant load, a uniformly distributed stress was generated on the surface of the sample.

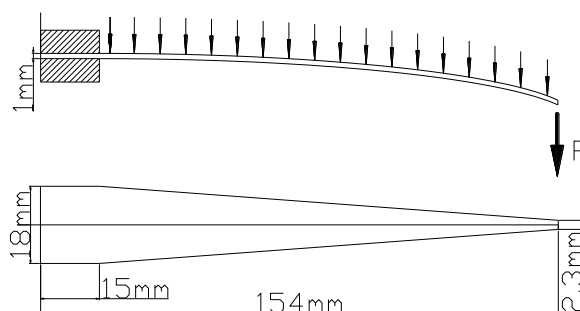


**Figure 1.** Sample size and the schematic of loading.

Four groups of immersion conditions were designed to compare the effect of each factor on the corrosion resistance of passive films. The experimental parameters and group numbers are listed in Table 2. A custom-made thermostat and clamping devices ensured that the experimental parameters were constant. The same 304 stainless steel was used as the material for the clamping and loading devices to avoid the impact of galvanic corrosion and other ions on the experimental results. The calculation of the mass of loads needs to consider the impact of solution buoyance. Deionized water and analytically pure NaCl were used to prepare the corrosion solution.

**Table 2.** Experimental groups and parameters.

Group number	1st group	2nd group	3rd group	4th group
Experimental conditions	90 °C + 100 MPa 3.5% NaCl solution	20 °C + 100 MPa 3.5% NaCl solution	90 °C + stress-free 3.5% NaCl solution	90 °C + 100 MPa deionized H <sub>2</sub> O without Cl <sup>-</sup>

After cleaning with ethanol, sonication and drying, the samples were characterized by X-ray photoelectron spectroscopy (XPS). A PHI 5700 ESCA System was used for the XPS analysis. The analysis was performed by using Al K $\alpha$  line (1486.6 eV) as the X-ray source under constant analyzer energy (CAE) mode. Wide scan: 187.85 eV. Narrow scan: 23.50 eV. Analysis area: 0.8  $\times$  2 mm. XPS Peak Fit 4.1 was used to analyze the data. The Shirley method was used for the background correction.

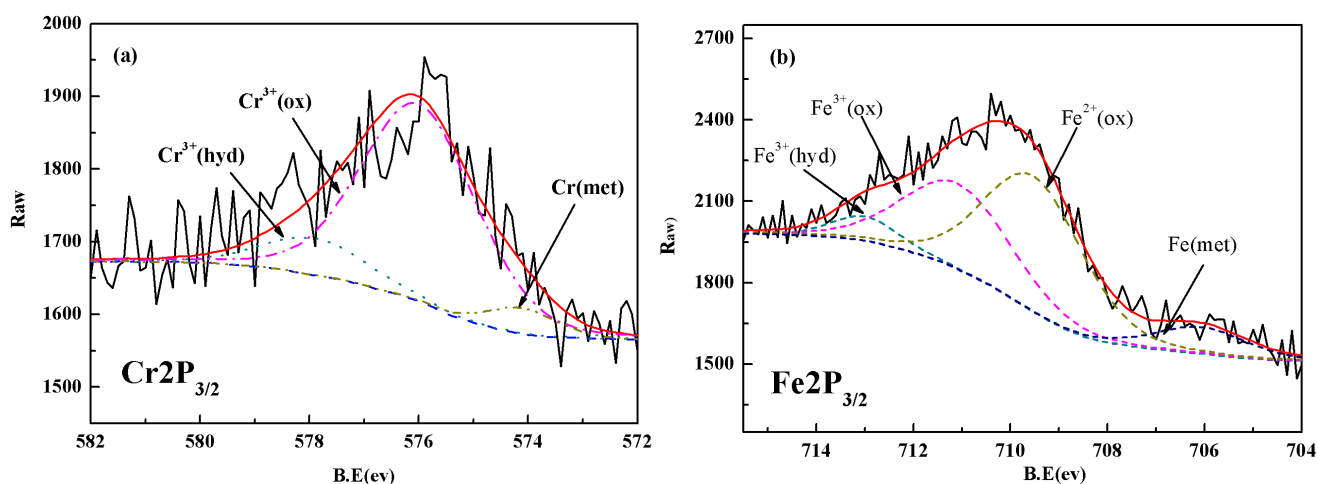
Atomic force microscopy (AFM) was used to characterize the surface morphology of the passive film. A Dimension Icon AFM from Bruker was used in tapping mode. Cantilever T: 1.5-2.5  $\mu$ m, L: 115-135  $\mu$ m, W: 25-35  $\mu$ m, F: 118-157 kHz, K: 5 N/m.

To understand the changing behaviors of the protection performance of the passive film, the immersed samples were characterized by electrochemical impedance spectroscopy (EIS). Before the EIS test, the samples were rinsed with deionized water and dried. The tests were performed at room temperature in a 3.5% NaCl solution. A three-electrode system was used in the EIS test, the reference electrode was Ag/AgCl electrode, the working electrode was the sample and the counter electrode was graphite electrode. The system was stabilized for 1800 s before the test.

### 3. RESULTS AND DISCUSSION

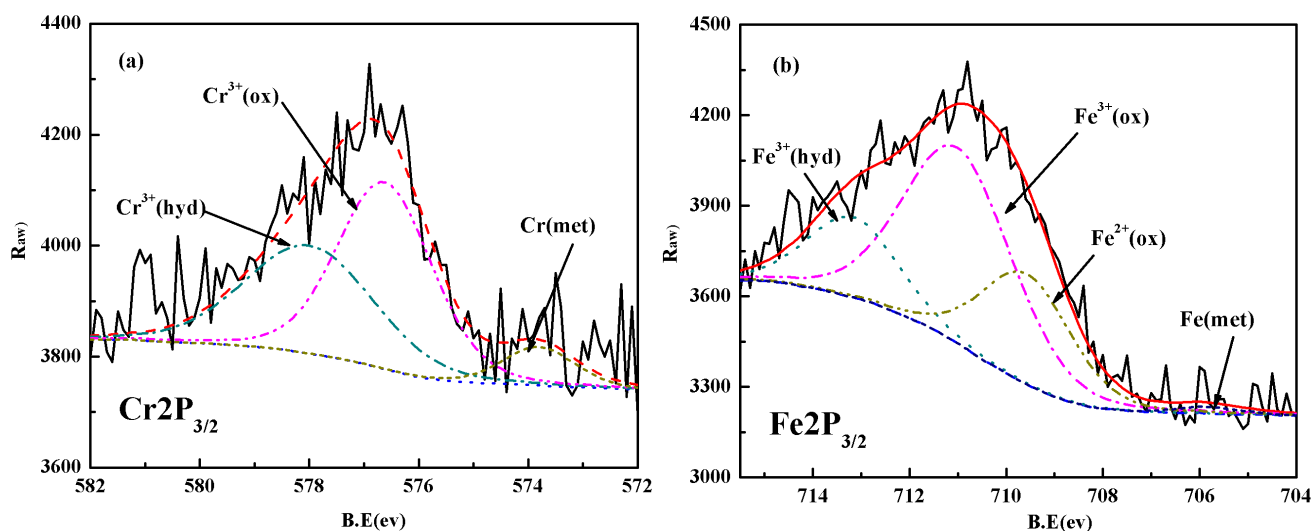
#### 3.1 Change in content of chemical compounds of passive films

The XPS spectrum of the passive film on the non-immersed sample is shown in Figure 2. The main chemical compounds in the passive film are the oxides and hydroxides of Fe and Cr [13-17], almost no Ni was detected [44]. The passive film consists of a two layer structure, an oxide-containing inner layer and a hydroxide-containing outer layer [9-12]. The measurement results show that the main compositions of the oxide layer are Cr<sup>3+</sup>(ox), Fe<sup>3+</sup>(ox) and Fe<sup>2+</sup>(ox), and that of the hydroxide layer are Cr<sup>3+</sup>(hyd) and Fe<sup>3+</sup>(hyd) [19,45]. The dense Cr<sub>2</sub>O<sub>3</sub> layer plays a crucial role in the corrosion resistance of the material [44-51].



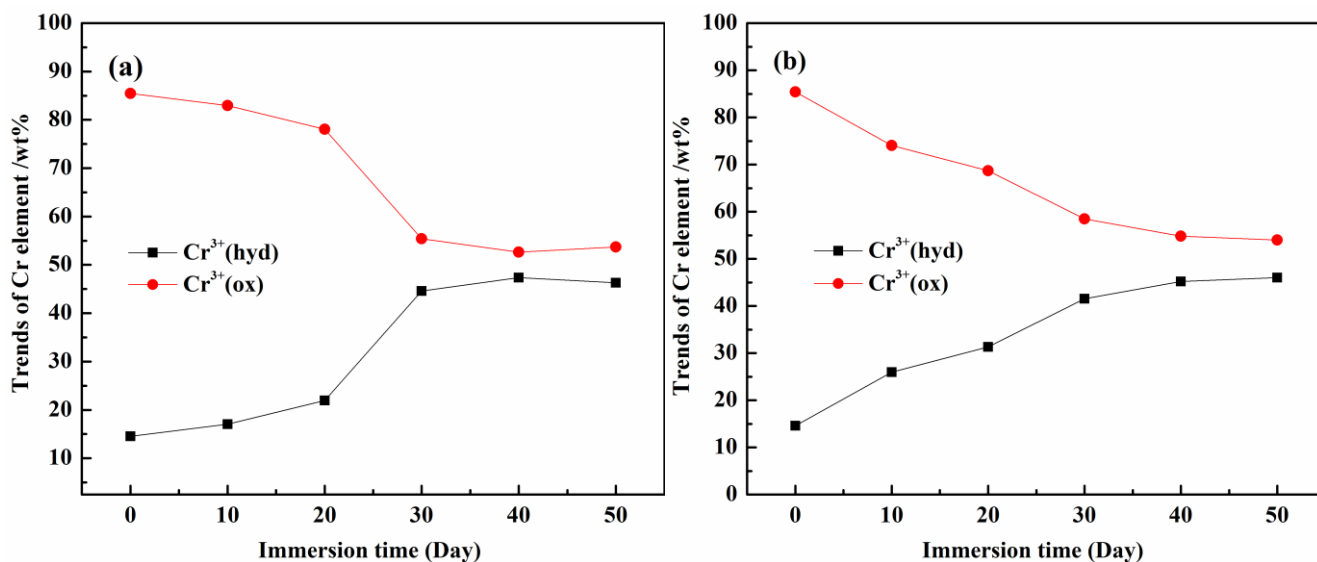
**Figure 2.** XPS spectra of Cr<sub>2</sub>p<sub>3/2</sub> and Fe<sub>2</sub>p<sub>3/2</sub> for non-immersed passive film: (a) Cr<sub>2</sub>p<sub>3/2</sub>; (b) Fe<sub>2</sub>p<sub>3/2</sub>.

Figure 3 shows the XPS spectra of the passive film on the sample immersed in 3.5% NaCl solution for 50 days (90 °C + 100 MPa). With increasing immersion time, there was no change in the chemical compositions of the passive film, but there was a significant change in the content of chemical compounds. Specifically, for the inner layer oxides, the content of Cr<sup>3+</sup>(ox) and Fe<sup>2+</sup>(ox) decreased, and that of Fe<sup>3+</sup>(ox) increased; for the outer layer hydroxides, the content of Cr<sup>3+</sup>(hyd) and Fe<sup>3+</sup>(hyd) increased.



**Figure 3.** XPS spectra of Cr<sub>2p<sub>3/2</sub></sub> and Fe<sub>2p<sub>3/2</sub></sub> for the passive film immersed in NaCl solution for 50 days (90 °C + 100 MPa): (a) Cr<sub>2p<sub>3/2</sub></sub>; (b) Fe<sub>2p<sub>3/2</sub></sub>.

The samples immersed for different times in the four groups were all characterized by XPS. Figure 4 summarizes the variation in the area ratio of Cr<sub>2p<sub>3/2</sub></sub> spectral line with time.



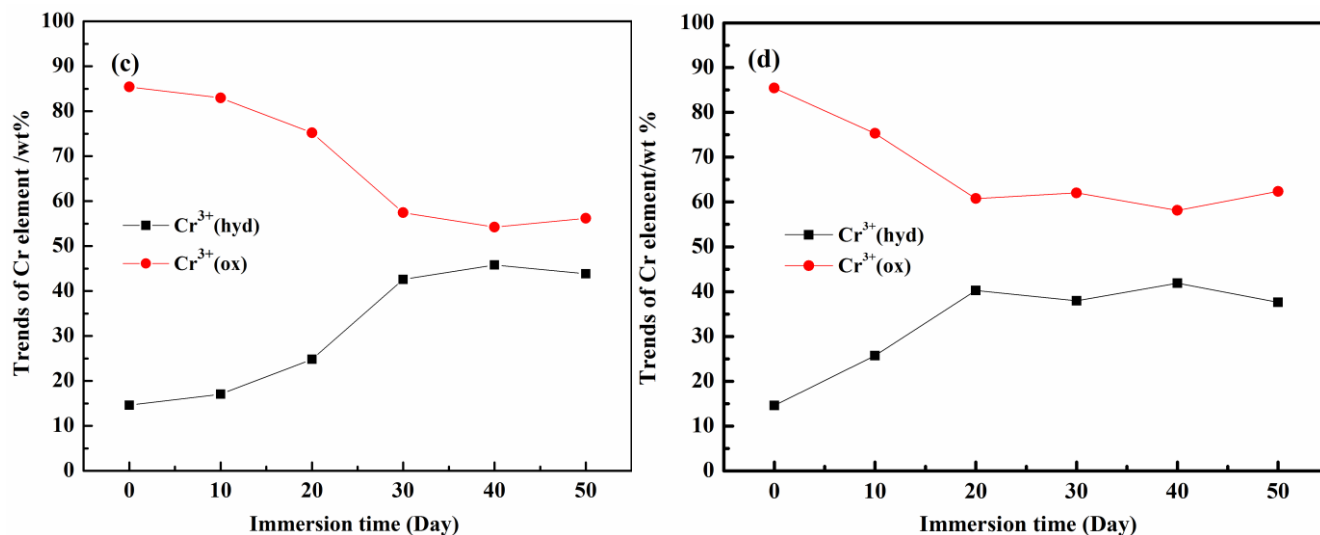


**Figure 4.** Area ratio of Cr<sub>2p<sub>3/2</sub></sub> spectral line in the passive film: (a) 90 °C + 100 MPa (NaCl solution); (b) 20 °C + 100 MPa (NaCl solution); (c) 90 °C (NaCl solution); (d) 90 °C + 100 MPa (H<sub>2</sub>O).

With increasing immersion time, for the Cr compounds in all passive films immersed at different conditions, the content of the inner layer oxide Cr<sup>3+</sup>(ox) decreased and that of the outer layer hydroxide Cr<sup>3+</sup>(hyd) increased. In addition, after immersion for 30 days, the content of Cr<sup>3+</sup>(ox) and Cr<sup>3+</sup>(hyd) in the passive film leveled off and stabilized.

The ratio of Cr<sup>3+</sup>(ox) to Cr<sup>3+</sup>(hyd) in the film of the four groups of samples all decreased from 8:1 before immersion to 11:9, 11:8, 11:9 and 3:2 of the stable state after immersion. The content of the Cr<sup>3+</sup>(ox) decreased relatively and that of the Cr<sup>3+</sup>(hyd) increased relatively. It can be found from the comparison of the 1st and 2nd groups that temperature has a certain effect on the dissolution rate of Cr<sup>3+</sup>(ox) [35,36]. Cr<sup>3+</sup>(ox) dissolves faster at low temperature. This is because although low temperature and stress can increase the content of adsorbed oxygen in the film [52], the presence of Cl<sup>-</sup> repulses adsorbed oxygen [39]. When the environmental potential was higher than that of  $V_{c \text{ film}}$ , Cl<sup>-</sup> preferably adsorbed to the surface of the passive film and the dissolution of Cr<sub>2</sub>O<sub>3</sub> was dominant [39]. This result agrees with the thermodynamic prediction by Kim [30] and the conclusion by Kuang[23]. The comparison of the 1st and 3rd groups shows that stress also improves the dissolution ratio of Cr<sub>2</sub>O<sub>3</sub>. The comparison of the 1st and 4th groups shows that in the absence of Cl<sup>-</sup>, Cr oxides can still be dissolved to solution (Figure 7(d)), but the dissolution ratio was lower [30,53,54]. This is because a large elastic stress enhances the dissolution reaction [52]. Cl<sup>-</sup> results in the generation of more defects in the passive film [20], which leads to the increase in the Cr<sub>2</sub>O<sub>3</sub> dissolution ratio. The adsorption of Cl<sup>-</sup> in the solution results in the increase in oxygen vacancy at the interface of the passive film. In turn, the cation vacancies are more easily generated with a faster rate [44].

Figure 5 summarizes the variation in the content of Fe compounds in the passive film with time. Before immersion, the ratio of Fe<sup>3+</sup>(ox) to Fe<sup>2+</sup>(ox) in the film was approximately 2:3. After immersion, the variation in the content of Fe compounds in the films of the four groups of samples was mainly as follows: the content of Fe<sup>3+</sup>(ox) and Fe<sup>3+</sup>(hyd) increased, and that of Fe<sup>2+</sup>(ox) decreased. With increasing immersion time, the ratio of Fe<sup>3+</sup>(ox) to Fe<sup>2+</sup>(ox) in the films of the 2nd, 3rd and 4th

groups of samples were relatively stable at approximately 4:1 (Figure 5(b), Figure 5(c) and Figure 5(d)), while that of the 1st group was approximately 5:3 (Figure 5(a)). This is because the adsorbed oxygen in the film can cause the Fe oxides to react ( $\text{FeO} \rightarrow \text{Fe}_2\text{O}_3$ ). Here, both temperature and stress promote the reaction [52]. The result is an increase in  $\text{Fe}_2\text{O}_3$  content and decrease in FeO content. For the Cl-containing solution, the Fe oxides can easily dissolve into solution, which also results in the decrease in  $\text{Fe}_2\text{O}_3$  content [37,38]. Concurrently, temperature and stress accelerate the dissolution of Fe oxides [52]. The generation and dissolution of  $\text{Fe}_2\text{O}_3$  will reach an equilibrium with immersion time [55]. However, the relative content of the  $\text{Fe}_2\text{O}_3$  in the 1st sample group was much smaller than that in the other three groups. This is because high temperature, stress, and  $\text{Cl}^-$  result in a much higher dissolution of Fe oxides in the immersion process than that in the other three groups.

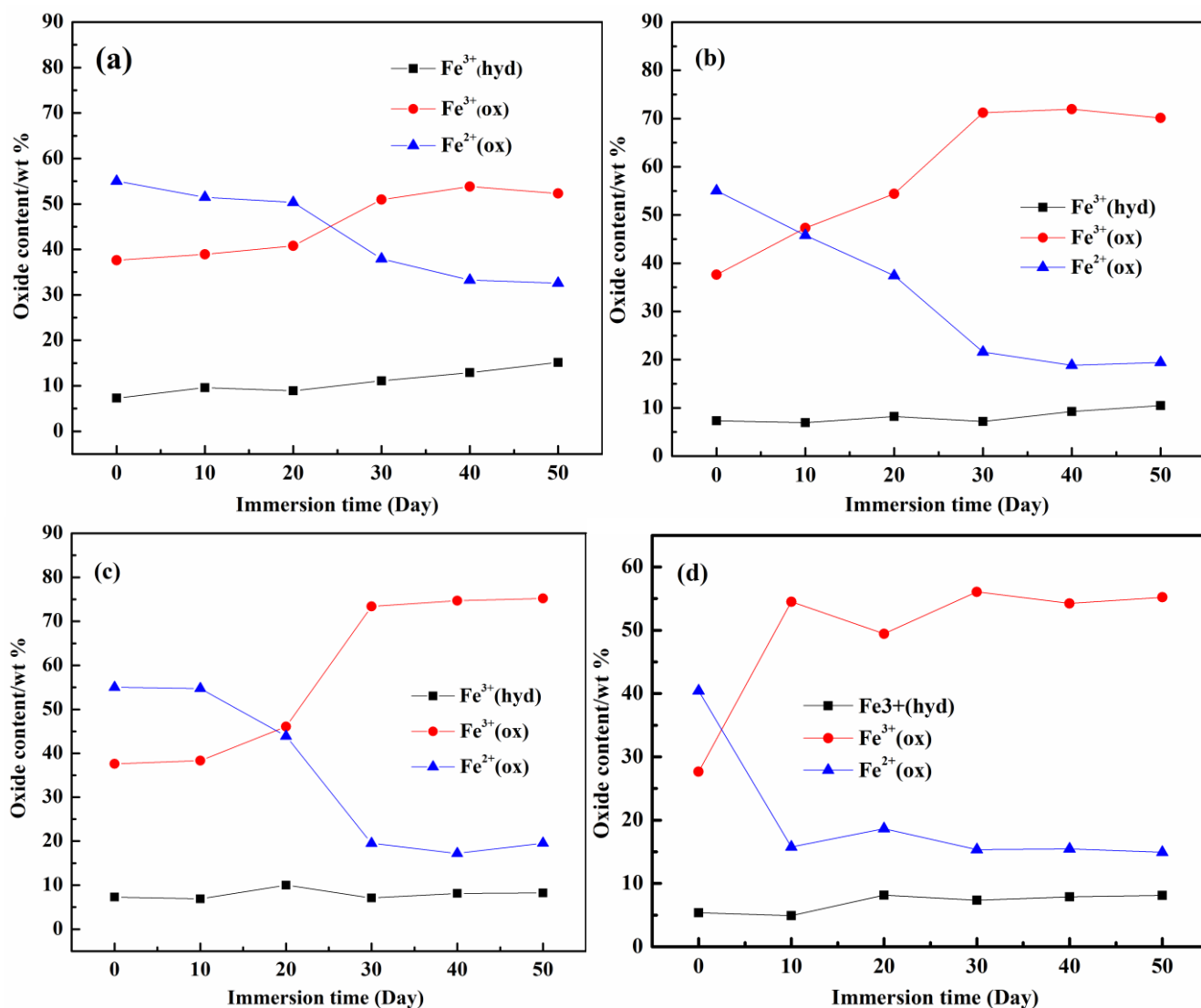


**Figure 5.** Area ratio of  $\text{Fe}2p_{3/2}$  spectral line in the passive film: (a) 90 °C + 100 MPa (NaCl solution); (b) 20 °C + 100 MPa (NaCl solution); (c) 90 °C (NaCl solution); (d) 90 °C + 100 MPa ( $\text{H}_2\text{O}$ ).

The slower increase in the content of outer layer  $\text{Fe}^{3+}(\text{hyd})$  in the passive film also confirms the presence of this process (Figure 5(a)). In the solutions without  $\text{Cl}^-$ , the content of the  $\text{Fe}_2\text{O}_3$  increased

rapidly, but its dissolution was restricted. The direct result is that it only takes 10 days for the generation and dissolution of Fe oxides in the film to reach equilibrium (Figure 5(d)), while that process takes almost 30 days for the other three groups.

Figure 6 summarizes the variation in the content ratio of the  $\text{Cr}^{3+}(\text{ox})$  in the passive film with time. Before immersion, the ratio of  $\text{Cr}^{3+}(\text{ox})$  to  $\text{Fe}^{3+}(\text{ox})$  to  $\text{Fe}^{2+}(\text{ox})$  was approximately 5:6:9 in the oxide layer and  $\text{Cr}^{3+}(\text{ox})$  accounts for approximately 25%. The ratio of the  $\text{Cr}_2\text{O}_3$  in the film exhibited a decreasing trend with increasing immersion time and stabilized at 12% to 25% after approximately 40 days. This is because the generation and dissolution of oxides in the film result in an increase in the total amount of oxides[23]. However, the faster increase in Fe oxides leads to a decrease in the percentage of the  $\text{Cr}_2\text{O}_3$ . In comparison, the percentage of the  $\text{Cr}_2\text{O}_3$  was higher in the 1st sample group than that in the other three groups. This is because in the 1st sample group, Fe in the passive film rapidly dissolves into solution [56,57]. In contrast, because of the extremely low exchange rate between the Cr(III) ions and ligands, the percentage of the  $\text{Cr}_2\text{O}_3$  is higher than that in the other sample groups [58].

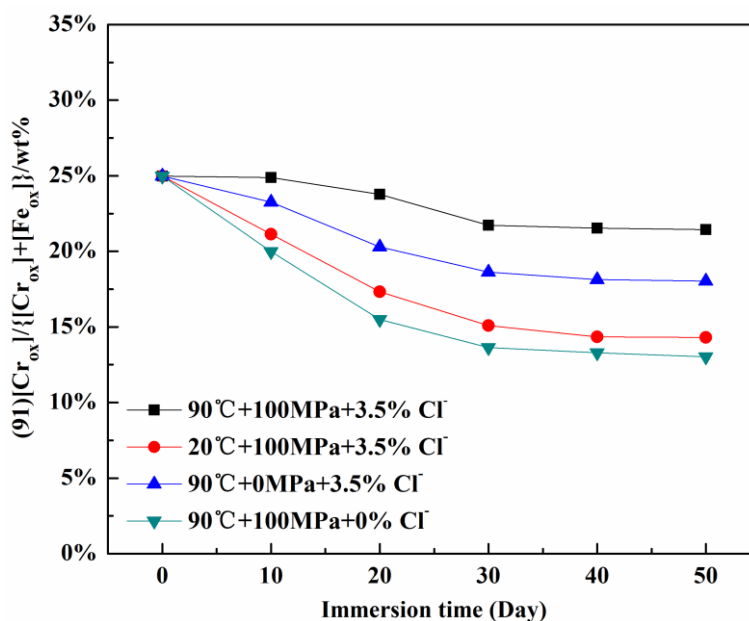
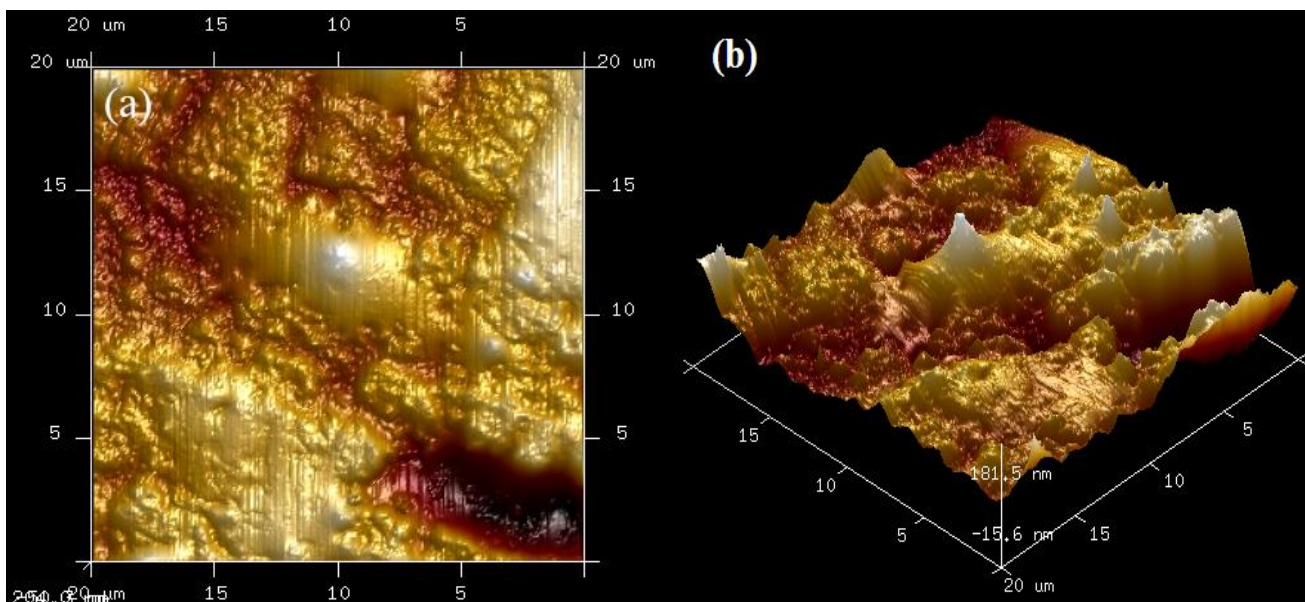


**Figure 6.** Variation in  $[\text{Cr}_{\text{ox}}]/\{[\text{Cr}_{\text{ox}}] + [\text{Fe}_{\text{ox}}]\}$  in the passive film with immersion time.

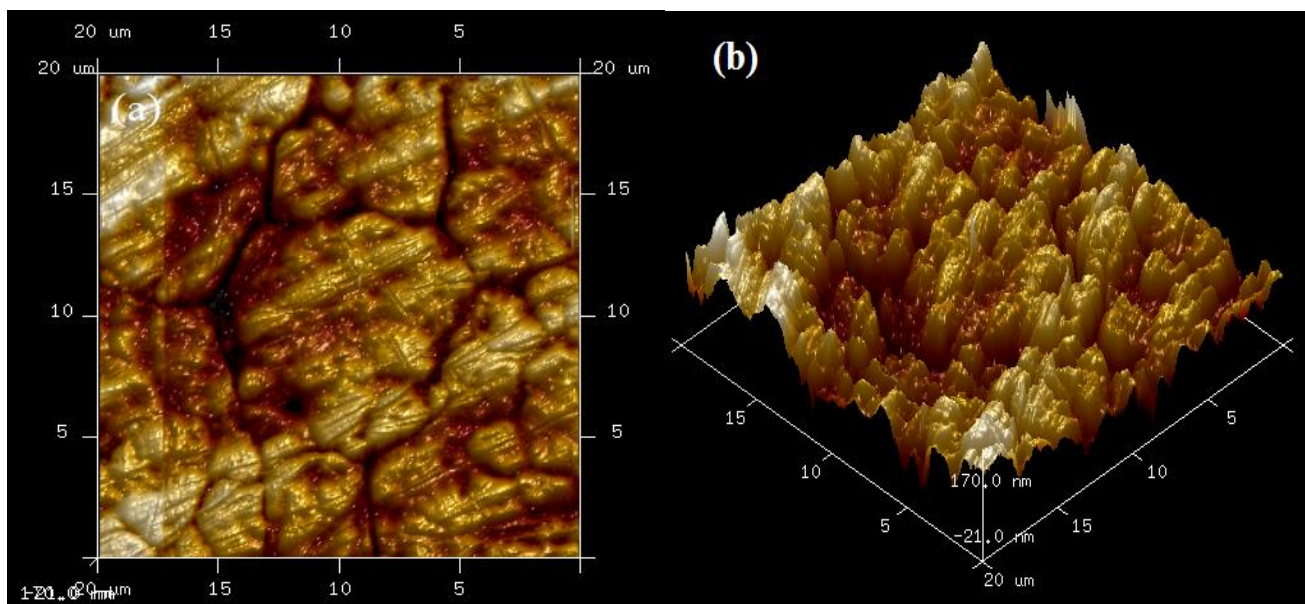
### 3.2 Changes in the surface morphology of passive films

Figure 7 shows that the surface morphology of the non-immersed passive film is continuous and dense. Figure 8 shows the AFM images of the passive film immersed in 3.5% NaCl solution for 10 days (90 °C + 100 MPa). “Corrosion grooves” (Figure 8(a)) appeared in the immersed passive film and had a peak-shaped convex appearance (Figure 8(b)). The comparison of the surface morphologies of the four groups of samples shows the appearance of “corrosion grooves” for all samples, which become deeper and longer and form a continuous network with increasing immersion time.

Figure 9 shows the SEM image of the non-immersed 304 stainless steel, the morphology and size of the grains are similar to that of passive film after corrosion (Figure 8). This comparison indicates that the “corrosion grooves” generated from immersion appear at the region of austenite grain boundary, the damage of the passive film occurs along the grain boundary.

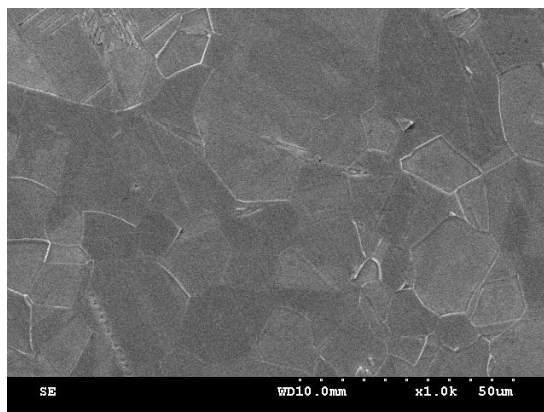


**Figure 7.** AFM images of non-immersed passive film: (a) 2D image; (b) 3D image.

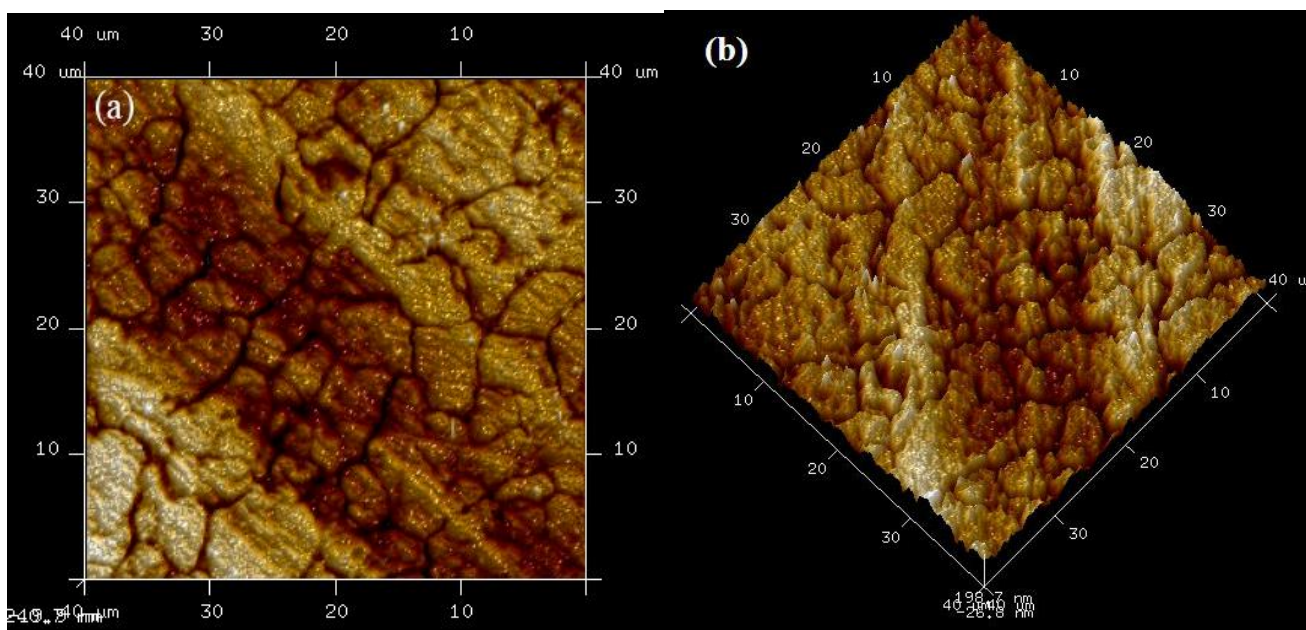


**Figure 8.** AFM images of the passive film immersed in 3.5% NaCl solution for 10 days (90 °C + 100 MPa): (a) 2D image; (b) 3D image.

The AFM analysis of the four groups of samples shows that after immersion for 10 days, all passive films experienced damage along the grain boundary. This is because  $\text{Cl}^-$  can adsorb to the surface of the passive film and then forms soluble chlorides with cations in the film, thus leading to the damage of the passive film. At the same time, there is a huge difference in the structural uniformity between the austenite grain and the grain boundary [15]. According to the poor-Cr theory, there is a 150-200 nm thick region of Cr-poor and Fe-rich at the grain boundary, because of the easy dissolution of Fe in  $\text{Cl}^-$ -containing solution, the passive film in this region is more easily damaged, thus the “corrosion grooves” appear along the grain boundary [16].



**Figure 9.** SEM image of the non-immersed 304 stainless steel.



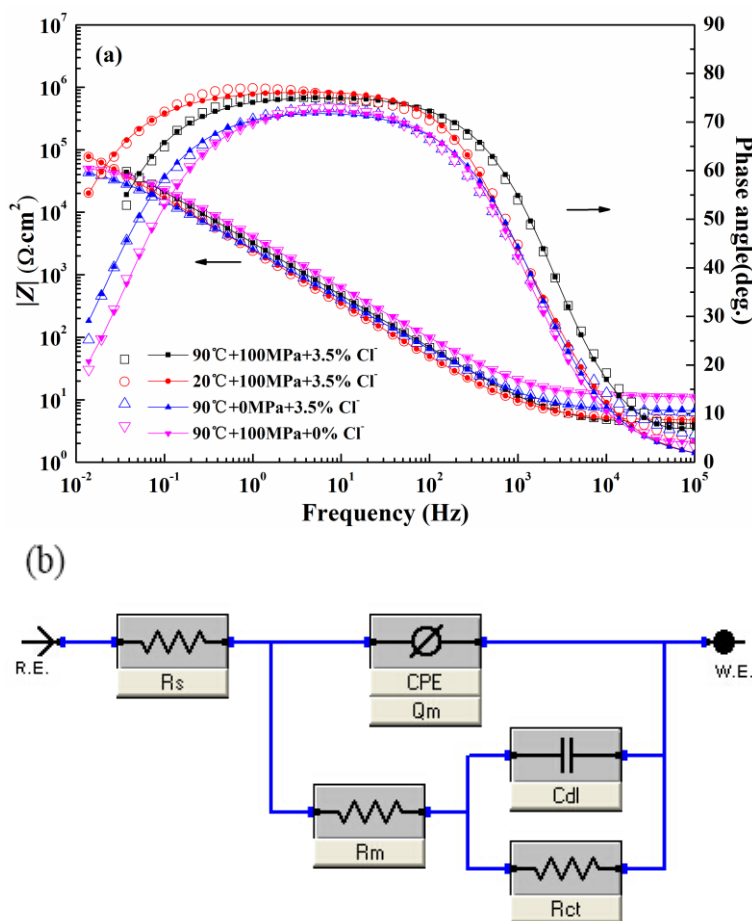
**Figure 10.** AFM images of the passive film immersed solution without  $\text{Cl}^-$  for 50 days ( $90^\circ\text{C} + 100\text{MPa}$ ): (a) 2D image; (b) 3D image.

Figure 10 shows the AFM image of the 4th sample group immersed in solution without  $\text{Cl}^-$  for 50 days. Surprisingly, damage along the interface of the grain boundary also occurred to the passive

film even in a Cl<sup>-</sup>-free environment. This is likely due to the combination of stress and high temperature resulting in a higher environmental potential than  $V_{c \text{ film}}$ , as a result, the dissolution of the passive film became the dominant mechanism. Based on the point defect model (PDM), stress and high temperature can accelerate the migration of cations in passive films [35,37]. The passive films become porous because of the dissolution of Fe and Cr even in Cl<sup>-</sup>-free environments [20]. In addition, at the grain boundary, the atomic arrangement is random, the dislocation density is high, and the internal stress from the phase transition is high. These factors all promote the dissolution of passive films in these regions.

The ion exchange between the substrate and the solution destroyed the weak links of the passive films at the grain boundary which further develop into continuous “corrosion grooves”. The ion exchange between the substrate and the solution that passes through the passive film undoubtedly causes damage to the dense Cr<sub>2</sub>O<sub>3</sub> layer and decreases the corrosion resistance of the material.

### 3.3 Electrochemical test



**Figure 11.** Bode plots of four groups of samples after immersion for 10 days and equivalent circuit model: (a) Bode plots; (b) Equivalent circuit model.

Electrochemical impedance spectroscopy (EIS) is an effective tool to investigate the corrosion resistance of passive film. The variation in film resistance can reflect the degree of integrity of the

passive film and its protection to the substrate. Figure 11 shows the Bode plots of the four groups of samples after immersion for 10 days and the equivalent circuit model, it can be seen that there are two time constants in the circuit,  $R_s$  represents the solution resistance,  $R_m$  represents the film resistance,  $R_{ct}$  corresponds to the charge transfer resistance,  $Q_m$  corresponds to the constant phase element (CPE) of the passive film and  $C_{dl}$  is the capacitance of the double electric layer [25].

Figure 12 shows the film resistance  $R_m$ . The  $R_m$  was significantly different for the four groups of samples after immersion for 10 days. When the immersion time was greater than 20 days, the  $R_m$  of the four groups of samples decreased from the initial value of 700  $\Omega$  to 25-50  $\Omega$ , and remained stable. These results indicate that the protection performance of the passive films rapidly decreased with increasing immersion time and ultimately reached a stable state when a similar damage was done to the passive film.

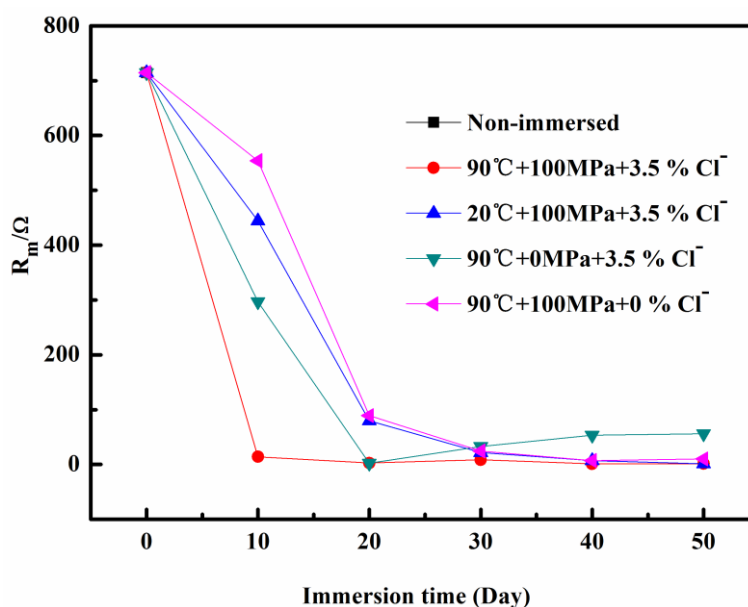


**Figure 12.** Variation in film resistance  $R_m$ .

The  $Cr_2O_3$  content in passive film [29], amorphous structure [34], defects and surface uniformity are the main factors responsible for the corrosion resistance of stainless steel. In the present study, the dense passive film became loose and porous with increasing immersion time, “corrosion grooves” appeared at the grain boundary and the protection performance of the passive film decreased [59]. The generation and dissolution of compounds result in a dramatic change to the outer layer (hematite) and inner layer (Cr-rich spinel) in the passive film compared to their initial states, thus causing the passive film to become loose and porous [23]. This reaction mainly occurs in the film at the surface of grains with a large area. The decrease in the percentage of  $Cr_2O_3$  and FeO and the increase in  $Fe_2O_3$  as shown in the XPS analysis further confirm the presence of this phenomenon. However, this is not the main reason for the dramatic decrease in protection performance. The height difference between the peak-shaped convex and the corrosion groove in the passive film already reached 200  $\mu m$ , which is far greater than the thickness of the passive film at approximately 10 nm

[22,36]. This result suggests that the passive films in the corrosion grooves are already very thin, and it is even possible that the metal substrate is already directly exposed to the solution. It is normally believed that the enrichment degree of the  $\text{Cr}_2\text{O}_3$  in the passive film plays a key role in its protection performance [21]. However, the percentage of the  $\text{Cr}_2\text{O}_3$  in the four groups of samples takes 40 days to reach a stable state, while it takes only 20 days for  $R_m$  to rapidly decrease from  $700 \Omega$  to below  $20 \Omega$  and remain stable. This is similar to the direct contact between the substrate of the material and the solution. These results indicate that the main factor for the protection performance of passive film is not the enrichment degree of the  $\text{Cr}_2\text{O}_3$  but the damage of passive film along the grain boundary. The damage of the surface of the passive film at the region of grain boundary is the main reason for the large decrease in protection performance.

When the depth of corrosion grooves was greater than the thickness of the passive film, the corrosion resistance of the passive film largely decreased. At this time, the impact of temperature, stress and  $\text{Cl}^-$  on the corrosion process is mainly reflected in the dissolution rate of substrate. Although the oxide content in the film increases with increasing immersion time, and the passive film becomes thicker accordingly, the thickness of the damaged passive film and the content of the  $\text{Cr}_2\text{O}_3$  can not accurately represent the protection performance of the passive film [60]. With the dissolution of the passive film, pitting corrosion will suddenly occur at certain locations of the substrate and ultimately lead to corrosion damage [60].

#### 4. CONCLUSIONS

The present study investigated the changes in chemical compositions, surface morphology and electrochemical properties of the passive film on 304 stainless steel under the combined effect of high temperature, stress and chloride ion. The content of each compound in the passive film for the four groups under experimental conditions changed with increasing immersion time, but the content ratio between each compound leveled off to a stable value. The underlying mechanism of the impact of each factor on the corrosion resistance is the promotion of the dissolution of the passive film at the surface of the grain boundary and the subsequent formation of “corrosion grooves”, which damages the surface of the passive films. The damage of the surface of the passive film at the grain boundary region is the primary reason for the large decrease in corrosion resistance. The decrease in film thickness at certain localities and the decrease in the film resistance  $R_m$  result in a large decrease in the corrosion resistance of the passive film and even the direct contact of the corrosion solution with the matrix of the material. Concurrently, the passive film almost loses its corrosion protection to the matrix. The impact of each factor on the corrosion process is primarily reflected in the dissolution rate of substrate.

#### References

1. C. Gaona-Tiburcio, F.H. Estupiñán-López, P. Zambrano-Robledo, J.A. Cabral M, C. Barrios - Durtewitz and F. Almeraya-Calderón, *Int. J. Electrochem. Sci.*, 11 (2016) 1080.
2. Adriana Samide, Gabriela Eugenia Iacobescu, Bogdan Tutunaru and Cristian Tigae, *Int. J.*

- Electrochem. Sci.*, 12 (2017) 2088.
3. M.C. Ramírez-López, L.A. Falcón-Franco, F.F. Curiel-López, P. Zambrano R, J.A. Cabral-Miramontes, C. Gaona-Tiburcio and F. Almeraya-Calderón, *Int. J. Electrochem. Sci.*, 12 (2017) 4928.
  4. G. Santiago-Hurtado, M.A. Baltazar-Zamora, J. Olguin-Coca, L.D. López L, R. Galván-Martínez, A. Ríos-Juárez, C. Gaona-Tiburcio and F. Almeraya-Calderón, *Int. J. Electrochem. Sci.*, 11 (2016) 2994.
  5. R.Y. Khaled, A.M. Abdel-Gaber and H.M. Holail, *Int. J. Electrochem. Sci.*, 11 (2016) 2790.
  6. E.F. Pieretti and M.D. Neves, *Int. J. Electrochem. Sci.*, 11 (2016) 3532.
  7. Y.A. Albrimi, Y.A. Addi, J. Douch, M. Hamdani and R.M. Souto, *Int. J. Electrochem. Sci.*, 11 (2016) 385.
  8. C. KÖSE and R. KAÇAR, *Int. J. Electrochem. Sci.*, 11 (2016) 2762.
  9. K. Asami, K. Hashimoto and S. Shimodaira, *Corros. Sci.*, 18 (1978) 151.
  10. V. Maurice, W.P. Yang and P. Marcus, *J. Electrochem. Soc.*, 145 (1998) 909.
  11. S. Fujimoto and H. Tsuchiya, *Corros. Sci.*, 49 (2007) 195.
  12. D.D. Macdonald and M.U. Macdonald, *J. Electrochem. Soc.*, 17 (1990) 2395.
  13. F.M. Delnick and N. Hackermann, *J. Electrochem. Soc.*, 126 (1979) 732.
  14. K. Azumi, T. Ohtsuka and N. Sato, *J. Electrochem. Soc.*, 134 (1987) 352.
  15. U. Stimming, J.W. Schultze and B. Bunsenges, *Phys. Chem.*, 8 (1976) 129.
  16. M.H. Dean and U. Stimming, *J. Electroanal. Chem.*, 228 (1987) 135.
  17. N.E. Hakiki, M.F. Montemor, M.G.S. Ferreira and M.D.C. Belo, *Corros. Sci.*, 42 (2000) 687.
  18. N. E. Hakiki, *Corros. Sci.*, 53 (2011) 2688.
  19. A. Fattahhosseini, M.A. Golozar, A. Saatchi and K. Raeissi, *Corros. Sci.*, 52 (2010) 205.
  20. N. Ramasubramanian, N. Preocanin and R.D. Davidson, *J. Electrochem. Soc.*, 132 (1985) 793.
  21. J. Xu, X.Q. Wu and E.H. Han, *Electrochim. Acta*, 71 (2012) 219.
  22. M.G.S. Ferreira, N.E. Hakiki, G. Goodlet, S. Faty, A.M.P. Simoes and M.D.C. Belo, *Electrochim. Acta*, 46 (2001) 3767.
  23. W.J. Kuang, X.Q. Wu and E.H. Han, *Corros. Sci.*, 63 (2012) 259.
  24. M. Bojinov, P. Kinnunen, K. Lundgren and G. Wikmark, *J. Electrochem. Soc.*, 152 (2005) B250.
  25. M. Bojinov, P. Kinnunen, G. Sundholm, *Corrosion*, 59 (2003) 91.
  26. D.J. Kim, H.C. Kwon and H.P. Kim, *Corros. Sci.*, 50 (2008) 1221.
  27. J.H. Ai, Y.Z. Chen, M.U. Macdonald and D.D. Macdonald, *J. Electrochem. Soc.*, 154 (2007) C43.
  28. J. Macak, P. Sajdl, P. Kucera, R. Novotny and J. Vosta, *Electrochim. Acta*, 51 (2006) 3566.
  29. I. Betova, M. Bojinov, P. Kinnunen, K. Lundgren and T. Saario, *J. Electrochem. Soc.*, 155 (2008) C81.
  30. Y. J. Kim, *Corrosion*, 51 (1995) 849.
  31. Y. J. Kim, *Corrosion*, 55 (1999) 81.
  32. T. Miyazawa, T. Terachi, S. Uchida, T. Satoh, T. Tsukada, Y. Satoh, Y. Wada and H. Hosokawa, *J. Nucl. Sci. Technol.*, 43 (2006) 884.
  33. C.S. Kumai and T.M. Devine, *Corrosion*, 63 (2007) 1101.
  34. M.F. Montemor, M.G.S. Ferreira, M. Walls, B. Rondot and M.C. Belo, *Corrosion*, 59 (2003) 11.
  35. Z.S. Smialowska, K.C. Chou and Z. Xia, *Corros. Sci.*, 32 (1991) 609.
  36. H. Sun, X.Q. Wu and E.H. Han, *Corros. Sci.*, 51 (2009) 2840.
  37. L.W. Niedrach and W.H. Stoddard, *Corrosion*, 42 (1986) 546.
  38. T.M. Angeliu and P.L. Andresen, *Corrosion*, 52 (1996) 28.
  39. H. Inagaki, A. Nishikawa, Y. Sugita and T. Tsuji, *J. Nucl. Sci. Technol.*, 40 (2003) 143.
  40. S.E. Ziemniak and M. Hanson, *Corros. Sci.*, 48 (2006) 2525.
  41. I. Betova, M. Bojinov, P. Kinnunen, K. Lundgren and T. Saario, *Electrochim. Acta*, 54 (2009) 1056.
  42. W.J. Kuang, X.Q. Wu, E.H. Han and J. Rao, *Corros. Sci.*, 53 (2011) 2582.

43. W.J. Kuang, X.Q. Wu, E.H. Han and L. Ruan, *Corros. Sci.*, 53 (2011) 1107.
44. I. Milosev and H.H. Strehblow, *J. Biomed. Res.*, 52 (2000) 404.
45. Q. Yang and J.L. Luo, *Electrochim. Acta.*, 45 (2000) 3927.
46. N.E. Hakiki, M.D.C. Belo, A.M.P. Simoes and M.G.S. Ferreira, *J. Electrochem. Soc.*, 145 (1998) 3821.
47. R.F.A. Jargelius-Pettersson and B.G. Pound, *J. Electrochem. Soc.*, 145 (1998) 1462.
48. I. Olefjord, B. Bronx and U. Jelvestam, *J. Electrochem. Soc.*, 132 (1985) 2854.
49. C. Calinski and H.H. Strehblow, *J. Electrochem. Soc.*, 136 (1989) 1328.
50. G. Lorang, M.D.C. Belo, A.M.P. Simoes, M.G.S. Ferreira, *J. Electrochem. Soc.*, 141 (1994) 3347.
51. N.D. Cristofaro, M. Piantini and N. Zacchetti, *Corros. Sci.*, 39 (1997) 2181.
52. M. Clarke, *Corros. Sci.*, 4 (1964) 372.
53. Y. Hemmi, Y. Uruma and N. Ichikawa, *J. Nucl. Sci. Technol.*, 31 (1994) 443.
54. W.J. Kuang, X.Q. Wu, E.H. Han and J. Rao, *Corros. Sci.*, 53 (2011) 3853.
55. R.W. Bosch and M. Vankeerberghen, *Electrochim. Acta*, 52 (2007) 7538.
56. R. Kirchheim, B. Heine, H. Fischmeister, S. Hofmann, H. Knote and U. Stolz, *Corros. Sci.*, 29 (1989) 899.
57. K. Asami and K. Hashimoto, *Corros. Sci.*, 19 (1979) 1007.
58. B.O. Elfstrom, *Mater. Sci. Eng.*, 42 (1980) 173.
59. A. Kocijan, C. Donik and M. Jenko, *Corros. Sci.*, 49 (2007) 2083.
60. R.H. Jung, H. Tsuchiya and S. Fujimoto, *Corros. Sci.*, 58 (2012) 62.

© 2018 The Authors. Published by ESG ([www.electrochemsci.org](http://www.electrochemsci.org)). This article is an open access article distributed under the terms and conditions of the Creative Commons Attribution license (<http://creativecommons.org/licenses/by/4.0/>).